

# A Distance-preserving Matrix Sketch

Leland Wilkinson<sup>1, 2</sup> and Hengrui Luo<sup>3</sup>

<sup>1</sup>H2O.ai, 2307 Leghorn St, Mountain View, CA 94043, USA, E-mail: leland.wilkinson@h2o.ai

<sup>2</sup>Department of Computer Science, University of Illinois at Chicago,

<sup>3</sup>Lawrence Berkeley National Laboratory, Berkeley, CA, 94720, USA, E-mail: hrluo@lbl.gov

March 7, 2022

## Abstract

Visualizing very large matrices involves many formidable problems. Various popular solutions to these problems involve sampling, clustering, projection, or feature selection to reduce the size and complexity of the original task. An important aspect of these methods is how to preserve relative distances between points in the higher-dimensional space after reducing rows and columns to fit in a lower dimensional space. This aspect is important because conclusions based on faulty visual reasoning can be harmful. Judging dissimilar points as similar or similar points as dissimilar on the basis of a visualization can lead to false conclusions. To ameliorate this bias and to make visualizations of very large datasets feasible, we introduce a new algorithm that selects a subset of rows and columns of a rectangular matrix. This selection is designed to preserve relative distances as closely as possible. We compare our matrix sketch to more traditional alternatives on a variety of artificial and real datasets.

*Keywords:* Matrix sketching, visualization, dimension reduction, Frobenius coefficient.

## 1 Introduction

For a real data matrix  $X_{np}$  of size  $n \times p$ , we assume that rows represent points and columns represent dimensions in a real metric space ( $\mathbb{R}^p$ ). We might be interested in identifying such features as outliers, duplicate points, anomalies, or unusual distributions. When  $n$  and  $p$  are moderate in size, we can use simple plots and statistical methods to explore such features. As these parameters increase, however, these simple tasks become unwieldy.

## 1.1 The Problem and Challenges

Suppose we wish to explore an  $n$  by  $p$  matrix of real numbers where  $n$  and  $p$  are quite large (say,  $n \approx 10^9$  and  $p \approx 10^4$ ). Unlike the situation where  $n$  and  $p$  are moderate, several obstacles prevent us from accomplishing our goal under large  $n$  and  $p$ .

- The data won't fit in memory. We can use a columnar distributed database, but this usually fails to deliver the response times users expect in an interactive exploratory environment Batch and Elmqvist (2017)
- Our potential display algorithms do not scale to a problem this size (Keim, 2000)
- The curse of dimensionality means that computing distances between points in high dimensional spaces is problematic. We can use random projections to alleviate the problem, but then we lose the ability to interpret dimensions.
- We cannot send big data "over the wire" in client-server environments where response time is important. We can compress or sample data, but this hampers our ability to detect outliers and other singular features.
- Plotting many points on display devices (even megapixel or 4K) produces a big opaque spot. We can use kernels, alpha-channel rendering, binning, and other methods to mitigate overlaps, but this impedes brushing and linking gestures.
- Projections often violate metric axioms – points close together in higher-dimensional space may be far apart in lower-dimensional projections. Conversely, points far apart in higher-dimensional space may be close together in a projection (Luo et al., 2020).
- Thousands of dimensions overwhelm multivariate displays such as parallel coordinates and scatterplot matrices. They run out of display "real estate."

## 1.2 Our Contribution

We address these challenges with a new algorithm for subsetting data matrices. We select a subset of rows and columns of  $X_{np}$  :

$$X_{np} \mapsto X_{mp} \mapsto X[a, b]_{mk},$$

where  $m \ll n$  and  $k \ll p$  and  $a$  is a row index array of length  $m$  and  $b$  is a column index array of length  $k$ . We restrict our selection of  $X_{mk}$  to be approximately *distance-preserving*, where distances between the rows of  $X_{mk}$  are linearly related to the distances between the corresponding rows of  $X_{mp}$ .

In sketching the rows in  $X_{np}$ , we collect points that are relatively close to each other. Our method depends on computing  $m$  Euclidean balls of radius  $r$  in  $p$ -dimensional space. We choose  $r$  to be as small as possible when reducing  $n$  to a manageable-sized  $m$ .

In subsequently sketching columns in  $X_{mp}$ , we produce a submatrix of  $X_{mp}$  based on  $k$  of its columns. We select these  $k$  columns such that distances between the  $m$  rows in  $X_{mk}$  linearly approximate the distances between the  $m$  rows in  $X_{mp}$ . Our hope is that this new submatrix  $X_{mk}$  is substitutable for  $X_{np}$  in visual analytic explorations. Although this is a lossy compression, we are able to retain pointers to the rows and columns of  $X_{np}$  that are not in  $X_{mk}$ . Consequently, we can employ our sketching algorithm as a preprocessor to interactive applications.

Using these two successive algorithms allows subsequent analysis of  $X_{mk}$  based on a representative subset of its original columns using frequency-weighted statistical models; the weights for each row of  $X_{mk}$  are derived from the number of points inside each of the  $m$  balls.

Figure 1 contains data on world universities from the `cwurData.csv` dataset at <https://www.kaggle.com/mylesoneill/world-university-rankings>. The table has been anonymized and consists of a subset of the original dataset. The red cells denote values retained by the row and column sketch algorithms, while the white cells are omitted. The figure shows an actual application of a sketching algorithm so that readers can see exactly what it does.

From the construction side, our algorithm has several distinctive aspects. First, it is scalable to very large datasets with moderate growth of complexity. Second, it

national_rank	quality_of_education	alumni_employment	quality_of_faculty	publications	influence	citations	patents	score
1	7	9	1	1	1	1	5	100
2	9	17	3	12	4	4	1	91.67
3	17	11	5	4	2	2	15	89.5
1	10	24	4	16	16	11	50	86.17
4	2	29	7	37	22	22	18	85.21
5	8	14	2	53	33	26	101	82.5
2	13	28	9	15	13	19	26	82.34
6	14	31	12	14	6	15	66	79.14
7	23	21	10	13	12	14	5	78.86
8	16	52	6	6	5	3	16	78.55
9	15	26	8	34	20	28	101	73.82
10	21	42	14	22	21	16	10	73.69
11	31	16	24	9	10	8	9	73.64
1	32	19	31	8	19	23	3	69.49
12	34	77	20	11	9	9	7	66.94
1	26	66	11	40	51	44	34	66.69
2	42	38	19	25	36	43	23	65.76
1	4	101	22	101	67	101	29	65.09
13	62	59	23	3	11	6	13	64.05
14	61	101	15	10	8	10	22	63.11
15	1	101	16	101	28	96	101	61.74
2	24	93	13	101	91	101	28	60.76
16	89	75	17	42	24	34	62	60.55
17	101	101	21	19	3	13	33	59.7
18	64	63	33	17	30	21	21	59.66

Figure 1: Matrix of university ratings.

works on streaming data and it is parallelizable, since updating rows and columns involves additive updates of distances. Third, our algorithm produces axis-parallel results suitable for visualization; it does not create composites of the input columns and retains interpretability of dimensions in the original dataset.

## 2 Related Work

We first discuss operations on rows (to reduce the number of points  $n$ ) and then discuss operations on columns (to reduce dimensionality of points  $p$ ). For general surveys of big data visualization methods, see (Unwin et al., 2007; Ali et al., 2016; Liu et al., 2017; Peña et al., 2017). For more detail on feature extraction and dimensionality reduction in visual analytics, see Guyon et al. (2006); Fekete and Plaisant (2002); Krause et al. (2016).

## 2.1 Reducing Rows

First, we introduce row-reducing methods that use the original rows in the reduced matrix, including sampling, clustering, squashing and coresets. Second, we introduce row-reducing methods that creates new representative rows in the reduced matrix through aggregation.

### 2.1.1 Sampling

Sampling from the original data matrix is one way of reducing the sample size  $n$ , or the number of rows of the data matrix. A well-chosen sub-sample can represent the original dataset and recover most of the features of the original dataset.

Sampling is not a general solution to our challenges, however. The main problem is that sampling tends to exclude statistical information in areas of low density, especially involving outliers. Unfortunately, these are the features one most wants to see when first exploring a dataset. Figure 2 illustrates this problem. In the rightmost panel of the figure, we see a simple random sample of a million point Gaussian dataset shown in the leftmost panel. Notice that the outermost points in the raw data plot of a million points do not show up in the sampling plot. The center panel shows our sketching algorithm applied to the same dataset. All the outermost points appear in this plot. And the overall density (a bivariate spherical normal distribution) is more accurately displayed in the central panel.

### 2.1.2 Clustering

Clustering has been used for decades to reduce a large set of points to a smaller, more tractable, set suitable for subsequent analysis. In this approach, individual points are replaced by their cluster centroids and the count of original points in each cluster is recorded and used in subsequent statistical and visual analytics.

The  $k$ -means algorithm is probably the most popular clustering algorithm used for this purpose. It partitions points in a space into  $k$  Voronoi cells. (clusters necessarily exist) or for clustering. In theory, all points in a cell are closer to the centroid of that

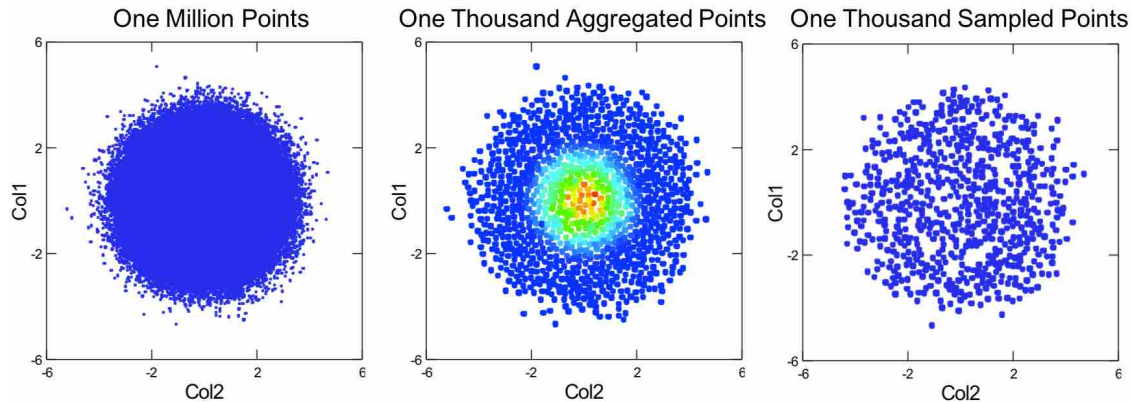


Figure 2: Scatterplots of a million spherical Gaussian (Normal) random numbers (left panel), a thousand aggregated points using the Matrix Sketch algorithm (middle panel), and a thousand randomly sampled points (right panel). We have used color to highlight points in the middle panel that have larger frequencies resulting from aggregation. The other two plots contain single points that all have a frequency of 1. We claim that the middle panel scatterplot is a more accurate visual representation of the million-points distribution in the left panel, especially with regard to points at the periphery of the distribution. In addition, the aggregated scatterplot in the middle panel lacks the holes in the right scatterplot that result from random sampling.

cell than they are to any other cell centroid. Also in theory,  $k$ -means centroids tend to lie in a subspace specified by a principal components decomposition (Ding and He, 2004a,b; Park et al., 2003).

We qualify these statements with the phrase “in theory” because there are many varieties of  $k$ -means algorithms; unfortunately, the theoretical solution is NP Hard (Mahajan et al., 2009). Furthermore, identifying the dimensionality of the embedding subspace is not easy. Most  $k$ -means algorithms require specifying  $k$  in advance of fitting. Ad hoc choices do not guarantee meaningful structure can be identified (Xie et al., 2016). And some measures of cluster-goodness appear to work well in many cases, but fail in others (Caliński and Harabasz, 1974; Rousseeuw, 1987)

### 2.1.3 Squashing

For the purpose of retaining statistical information when  $n$  is large, DuMouchel and colleagues coined the term DataSquashing to describe algorithms that attempt to preserve statistical information when “flattening” flat files (DuMouchel et al., 1999).

Other similar approaches are reviewed in DuMouchel (2002). These methods work well for certain classes of distributions. They do not claim to be an overall solution to the problem when  $n$  is large, however.

#### 2.1.4 Coresets

For the purpose of visualization with geometric properties retained, Coresets involve finding a subset of points (rows of a dataset or vertices of a graph) that can be used in subsequent analytics or visualizations. Coresets are often used in shape estimation from point sets or vertex-edge graphs. There are many algorithms that fall within this class of problems (Agarwal et al., 2005).

#### 2.1.5 Aggregation

An alternative way of reducing the sample size is aggregating. Unlike sampling, aggregating does not necessarily select data points from the original dataset. Instead, it creates new representative data points based on the topology of the original dataset.

**1-dimensional Aggregation** The simplest, and probably oldest, form of aggregation involves a single variable. Histogramming is a simple method for aggregating values on a single variable.

1. Choose a small bin width ( $k = 500$  bins works well for most display resolutions).
2. Bin rows in one pass through the data.
3. When finished, average the values in each bin to get a single centroid value.
4. Delete empty bins and return centroids and counts in each bin.

An alternative one-dimensional aggregation method is based on dot plots (Wilkinson, 1999). Instead of choosing bins of equal width, we stack dots of radius  $r$  to represent points. We choose  $r$  to result in  $k$  stacks; smaller values of  $r$  yield more stacks. This algorithm is a one-dimensional version of the row sketching algorithm introduced in this paper. *Vector quantization* involves dividing a set of points into exclusive subsets. It is equivalent to histogramming with equal or unequal bin widths.

**2-dimensional Aggregation** Two-dimensional aggregation is a simple extension of the one-dimensional histogram algorithm. We take a pair of columns to get  $(x,y)$  tuples and then bin them into a  $k \times k$  rectangular grid. After binning, we delete empty bins and return centroids based on the averages of the coordinates of members in each grid cell.

Although a little more expensive to compute, *hexagonal bins* (Kosugi et al., 1986; Carr et al., 1987) are preferable to rectangular binning in two dimensions. With square bins, the distance from the bin center to the farthest point on the bin edge is larger than that to the nearest point in the neighboring bin. The square bin shape leads to local anisotropy and creates visible Moiré patterns. Hexagonal bins reduces this effect.

The surface of a sphere is a two-dimensional object. Consequently, we can bin  $(x,y)$  tuples on a globe. It seems reasonable to select hexagons to tile the globe, but a complete tiling of the sphere with hexagons is impossible. Compromises are available, however. Carr et al. (1997) and Kimerling et al. (1999) discuss this in more detail.

**$n$ -dimensional Aggregation** Unfortunately, high-dimensional aggregation cannot be accomplished through simple extensions of 2D binning. Tiling high-dimensional spaces is problematic (Sayood, 2012).

A number of papers attack the high-dimensional problem through 2D slices of the  $n$ D data. One of the best applications is also one of the oldest: the Grand Tour (Asimov, 1985). A more recent implementation follows a different route through space based on Hamiltonian paths (Hurley and Oldford, 2011). Both smoothly animate the path of 2D projections and give users the chance to control the process. But a collection of 2D binnings across an  $n$ D space does not accurately reflect or necessarily reveal joint structures in  $n$  dimensions. Other subspace aggregations share similar problems. Preaggregated hash tables, for example, can improve response time from databases, but they are useful mainly for low-dimensional tables (Pahins et al., 2016). Other approaches include machine-guided subspace views (Xie et al., 2009; Krause et al., 2016).



## 2.2 Reducing Columns

In this section, we introduce column-reducing methods that output the original columns in the reduced matrix. Then we introduce column-reducing methods that creates new representative columns in the reduced matrix through projections.

### 2.2.1 Feature Extraction

Feature extraction involves finding a subset of features (columns) that can be used in subsequent analytics or visualizations. Most of these methods involve cluster analysis (in one form or another) or principal components (Guyon et al., 2006; Dy and Brodley, 2004; Friedman and Meulman, 2004; Cheng et al., 1999). These two classes of analytics are used to decompose variation in order to identify columns most contributing to that subspace variation.

Unlike projection methods we will introduce below, and like matrix sketching, these approaches aim to produce sets of original variables rather than composites so that interpretation of results can be made in the original data space. However, some feature extraction methods may not depend on statistical procedures like cluster analysis or *PCA* and sometimes they do not rest on assumptions concerning the distribution of the data.

### 2.2.2 Projection

A projection, in the restricted sense employed in most visual analytics, is the mapping of a set of points in  $p$  dimensions to a subspace of  $k$  dimensions. This kind of projection can involve a linear map (as with principal components) or a nonlinear map (as in manifold learning). These methods can also be used for modeling (as in unsupervised learning) or as preliminary steps in feature engineering. (Cavallo and Demiralp, 2018; Tatu et al., 2011)

**Linear projection** Principal Component Analysis (PCA) is among the most popular linear dimension reduction methods. The original statistical algorithm for computing

principal components (Pearson, 1901; Hotelling, 1933), begins with a covariance matrix  $S$  derived from the product of a column-centered  $X$  matrix and its transpose and computes an eigendecomposition of that matrix (equation 1),

$$S = X^T X / n = V D V^T \quad (1)$$

where the  $D$  is a diagonal matrix of eigenvalues and  $V$  is a matrix of eigenvectors. The PCA projects the data matrix linearly to the principal component directions.

Principal components were originally designed for multivariate normally distributed points with zero mean. They can still be useful for snapshots of other types of data. More recent methods like nonlinear principal components (Hsieh, 2009) and sparse principal components (Zou et al., 2006) are more flexible. The Singular Value Decomposition (SVD) works directly on a rectangular matrix. It is a generalization of the Principal Components decomposition, as equation 2 shows. The SVD algorithm bypasses the need for computing the covariance matrix  $S$ .

$$\begin{aligned} X &= U D V^T \\ X^T X &= (U D V^T)^T U D V^T = V D^T U^T U D V^T = V D^2 V^T \end{aligned} \quad (2)$$

Linear projections may not preserve metrics, and therefore geometry of the dataset (Luo et al., 2020). A major group of existing visualization procedures when  $p$  is large make use of dimension reduction via linear projections. However, projections often violate metric axioms – points close together in higher-dimensional space may be far apart in lower-dimensional projections. Conversely, points far apart in higher-dimensional space may be close together in a projection.

**Nonlinear Projection.** The development of nonmetric multidimensional scaling of symmetric similarity or dissimilarity matrices in the 1960’s (Shepard, 1962a,b; Kruskal, 1964) led to interest in projecting rectangular data into low-dimensional subspaces.

Carroll and Chang at Bell Laboratories developed a topological embedding program called *PARAMAP* (Shepard and Carroll, 1966). Since then, numerous researchers have developed models and programs along similar lines (Tenenbaum et al., 2000; Belkin and Niyogi, 2003; Roweis and Saul, 2000; van der Maaten and Hinton, 2008; McInnes et al., 2018).

These *manifold learning* methods, linear or nonlinear, assume points lie near a  $k$ -dimensional manifold embedded in a subspace of the  $p$ -dimensional ambient space and they assume the conditional distribution of the distances of points to the manifold (residuals) is random and relatively homogeneous. Unlike principal components, however, manifold learning methods do their best when the distribution of errors is close to a nonlinear manifold; they do not do well with data containing substantial error.

Nonlinear projections, although attempting to preserve local geometric features, can also violate metric axioms, which can be harmful. For example, a low-dimensional map from a higher-dimensional space that induces viewers to infer that *dissimilar* points in the higher-dimensional space are *similar* can lead to false conclusions. Conversely, a low-dimensional map from a higher-dimensional space that induces viewers to infer that *similar* points in the higher-dimensional space are *dissimilar* can lead to false conclusions. This is a commonly-expressed warning in the manifold learning community (Wattenberg et al., 2016).

### 2.3 Reducing Rows and Columns

Matrix Sketching (Liberty, 2013; Woodruff, 2014) reduces rows or columns or both simultaneously. Our algorithm is a form of matrix sketching. In general, matrix sketching represents a matrix  $X$  through a sketch matrix  $\tilde{X}$  such that the error  $\|X^T X - \tilde{X}^T \tilde{X}\|$  is relatively small.

We exemplify the matrix sketching method using CUR decomposition. The *CUR* decomposition is similar to the Singular Value Decomposition (*SVD*) (Stewart and Stewart, 1998; Drineas et al., 2008):

$$X = CUR \tag{3}$$

For  $X_{np}$  the  $CUR$  components are dimensioned as  $C_{nk}$ ,  $U_{km}$  and  $R_{mp}$ , where  $1 \leq m \leq n$  and  $1 \leq k \leq p$ . This restriction forces equation 3 to be an approximation rather than an isometry. Some  $CUR$  algorithms are relatively efficient (Drineas et al., 2008); their time performance can be  $O(np^2)$ .

The same kind of rank reduction can be achieved with an  $SVD$ . Unlike  $SVD$ s, however, the matrices  $C$  and  $R$  are subsets of the rows and columns of  $X$  rather than linear combinations of them. This feature of  $CUR$ , shared by our matrix sketching algorithm, is distinctive.

However,  $CUR$  differs from our algorithm in several respects. First,  $CUR$  outputs three matrices while ours outputs one. Second, the  $CUR$  algorithm leaves  $n$  and  $p$  unchanged in the  $C$  and  $R$  matrices. By contrast, our algorithm reduces  $n$  and  $p$  to  $m$  and  $k$  respectively. Third, many  $CUR$  algorithms involve random sampling; ours is deterministic. For a more general survey of matrix decompositions suited to high-dimensional data, see (Halko et al., 2011).

### 3 A New Matrix Sketching Algorithm

Our matrix sketch is based on two associated algorithms. We first consider sketching rows to reduce  $n$ . Then we consider sketching columns to reduce  $p$ .

#### 3.1 Sketching Rows

Our algorithm for reducing the number of rows is related to a greedy approximate solution to the  $k$ -center problem (Cormode and McGregor, 2008):

Given  $n$  points in  $p$ -dimensional metric space and an integer  $k \leq n$ , find the minimum radius  $r$  and a set of balls of radius  $r$  centered on each of  $m$  points such that all  $n$  points lie within the union of these balls.

Instead of conditioning on  $k$ , however, we condition on  $r$  and denote the final number of centers to be  $m$  in following discussion. Our algorithm is derived from a variant of the Leader clustering algorithm, which is described in (Hartigan, 1975). Algorithm 1 shows the rows sketching algorithm.

---

**Algorithm 1:** Rows Algorithm

---

**Data:**  $X_{n,p}$  (data matrix)  
**Input:**  $r = .25/(\log n)^{1/p}$  (default value)  
1 EuclideanDistance ( $a, b$ ) is a Euclidean distance function  
**Result:** *exemplars* (list of ball centers), *members* (list of lists)  
2 **begin**  
3     Normalize columns of  $X$  so each is bounded by  $[0,1]$   
4      $m = 1$   
5      $row$  (array of length  $p$ ) = first row of  $X$   
6     *exemplars* = new list, initialized to contain  $row$   
7     *members* = new list of lists, initialized to contain empty list  
8 **end**  
9 **for**  $i = 1, \dots, n$  **do**  
10     *newExemplar* = *true*  
11      $row = X[i, \cdot]$  ( $i$ th row of  $X$ )  
12     **for**  $j = 1, \dots, m$  **do**  
13          $d = \text{EuclideanDistance}(row, exemplars[j])$   
14         **if**  $d < r$  **then**  
15             add  $i$  to *members*[ $j$ ]  
16             *newExemplar* = *false*  
17             **break**  
18         **end**  
19     **end**  
20     **if** *newExemplar* **then**  
21          $m = m + 1$   
22         add  $row$  to *exemplars*[ $m$ ]  
23         add new list to *members*[ $m$ ], initialized with  $i$   
24     **end**  
25 **end**

---

### 3.1.1 Notes on Rows Algorithm

1. The default value of  $r$  is designed roughly to be below the expected value of the distances between  $n(n-1)/2$  pairs of points distributed randomly in a  $p$  dimensional unit hypercube. Increase  $r$  to produce fewer exemplars, decrease to produce more.
2. The *exemplars* list contains a list of row values representing points defining an exemplar neighborhood.
3. The *members* list of lists contains one list of indices for each exemplar pointing to members of that exemplar's neighborhood.
4. The Leader algorithm (Hartigan, 1975) creates exemplar-neighborhoods in one pass through the data. It is equivalent to centering balls in  $p$  dimensional space on points in the dataset that are considered to be exemplars. Unlike  $k$ -means clustering, the Leader algorithm
  - (a) centers balls on actual data points rather than on centroids of clusters,
  - (b) constrains every ball to the same radius rather than allowing clusters to have different diameters,
  - (c) involves only one pass through the data rather than iterating to convergence via multiple passes,
  - (d) produces many balls rather than a few clusters.
5. Normalizing columns of  $X$  follows conventional practice in supervised learning, especially clustering. We are using Euclidean balls (not ellipses) because we want to ensure that distances are computed isotropically.
6. If there are enough columns for the curse of dimensionality to become a problem, we can preprocess the data using random projections (Johnson and Lindenstrauss, 1984) to reduce the total number of columns used for calculation of distances between points.
7. In rare instances, the resulting exemplars and members can be dependent on the order of the data, but not enough to affect the description of the joint density of points because of the large number of exemplars produced. We are characterizing

a high-dimensional density by covering it with many small balls. Even relatively tight clusters produced by a clustering algorithm will be chopped into pieces by the Leader algorithm.

8. The time complexity of Algorithm 1 is  $O(nmp)$ .

Figure 3 shows a schematic depicting a 2D implementation of our algorithm.

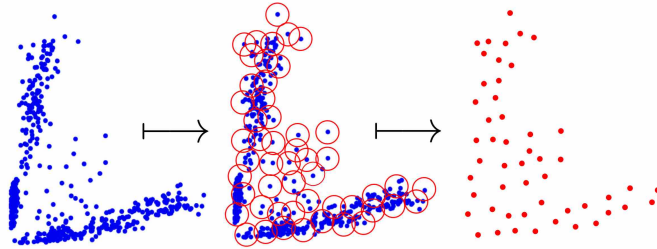


Figure 3: Visualization of the row sketching algorithm in a 2D space.

### 3.1.2 Performance of Rows Algorithm

A consequence of aggregating rows is that statistics on the aggregates must include frequency weighting. This requirement rules out some statistical libraries that do not incorporate frequencies. Most statistical packages for survey analysis, for example, incorporate frequency weighting in their basic statistics (or, in the case of SAS or SYSTAT or STATA, everywhere).

Table 1 is based on the million Gaussians dataset used for Figure 2. The three stub panels show the results of computing basic statistics on three different datasets. The Sketch Dataset uses our row sketching algorithm and the Random Sample uses a simple random sample to extract 200 rows from the million. Both row-reducing methods do quite well overall, but there is a striking difference. The row sketching algorithm yields the maxima and minima of the raw dataset, but the Sample method does not. In short, the row sketching algorithm, coupled with frequency-weighted formulas, does quite well on basic statistics.

	<b>X</b>	<b>Y</b>	<b>Z</b>
<b>Original Dataset</b>			
m	1,000,000	1,000,000	1,000,000
n	1,000,000	1,000,000	1,000,000
Min	-4.683	-5.208	-5.184
Max	5.061	4.702	4.832
Mean	-0.001	0.000	0.001
Median	0.000	0.001	0.001
SD	1.000	1.000	1.001
<b>Sketch Dataset</b>			
m	200	200	200
n	1,000,000	1,000,000	1,000,000
Min	-4.683	-5.208	-5.184
Max	5.061	4.702	4.832
Mean	0.003	0.008	0.008
Median	-0.104	0.076	0.031
SD	1.095	1.114	1.130
<b>Random Sample</b>			
m	200	200	200
n	1,000,000	1,000,000	1,000,000
Min	-2.916	-2.539	-2.628
Max	2.950	2.513	3.002
Mean	-0.049	-0.020	-0.015
Median	-0.048	0.013	0.010
SD	1.011	0.939	1.046

Table 1: Original vs. Sketch and Random Sample of a Million Gaussians

### 3.2 Sketching Columns

Algorithm 2 contains the columns sketching algorithm. Our column sketching algorithm is based on a variant of greedy forward feature selection with a Frobenius coefficient to measure similarity between distance matrices.



---

**Algorithm 2:** Columns Algorithm

---

**Data:**  $X_{m,p}$  (data matrix sketched with algorithm 1)  
**Input:**  $maxCorrelation = .95$  (default value)

- 1  $sum(a, b)$  is an element-wise sum function on two arrays
- 2  $dist(X_{m,p})$  produces an  $m(m-1)/2$  array of squared distances
- 3  $FrobeniusCorrelation(a, b) = (a \cdot b) / (\|a\| \|b\|)$

**Result:**  $selectedCols$  (list of selected columns)

- 4 **begin**
- 5     Normalize columns of  $X$  so each is bounded by  $[0, 1]$
- 6      $correlation = 0.0$
- 7      $selectedCols =$  list of selected columns initialized empty
- 8      $previousColDist = m(m-1)/2$  length array of zeros
- 9      $allColDist = m(m-1)/2$  array of distances from  $dist(X_{:,j})$
- 10 **end**
- 11 **while**  $correlation < maxCorrelation$  **do**
- 12      $bestColumn = 0$
- 13      $bestCorrelation = 0.0$
- 14      $previousBestCorrelation = 0.0$
- 15     **for**  $j = 1, \dots, p$  **do**
- 16         **if**  $j \notin selectedCols$  **then**
- 17              $jColDist = dist(X[:, j])$
- 18              $cumColDist = sum(jColDist, previousColDist)$
- 19              $correlation = FrobeniusCorrelation(cumColDist, allColDist)$
- 20             **if**  $correlation > bestCorrelation$  **then**
- 21                  $bestColumn = j$
- 22                  $bestCorrelation = correlation$
- 23             **end**
- 24     **end**
- 25     **end**
- 26      $bestColDist = dist(X[:, bestColumn])$
- 27      $previousColDist = sum(bestColDist, previousColDist)$
- 28     add  $bestColumn$  to  $selectedCols$
- 29      $previousBestCorrelation = bestCorrelation$
- 30 **end**

---

### 3.2.1 Notes on Columns Algorithm

1. Normalizing columns of  $X$  follows conventional practice in supervised learning, especially clustering. We may choose to retain the original scales when they do not differ substantially.

2. Our algorithm accumulates squared distances in *cumColDist* on each iteration over  $p$ . This saves time by confining distance computations at each step to a pair of column arrays rather than to a matrix of columns. Since squared distances are additive, we need to compute only one-dimensional distances in each step and cumulate them with previously-computed squared distances.
3. The time complexity of Algorithm 2 is  $O(kmp)$ .

### 3.2.2 Performance of Columns Algorithm

We present in this section various approaches to evaluating the performance of the columns algorithm. Some of these are designed to illustrate differences from other algorithms rather than overall effectiveness.

**Distance Preservation.** The loss functions and error bounds for many of these projection methods are variously based on the discrepancy between the coordinates of the points in the low-dimensional embedding space and their coordinates in the higher-dimensional residual space. The loss function for *Matrix Sketch*, by contrast, is based on the correlation between the distances reproduced by the sketch matrix and the original distances between points. In short, most popular projection methods (with the exception of multidimensional scaling, which is challenging to apply on large datasets (Paradis, 2018)) are not distance-preserving.

We can compare the distance-preserving capabilities of several column-reducing algorithms. Figure 4 shows a SPLOM of the column sketch algorithm vs. several other projection methods. The data are taken from the gene expression dataset used in Figure 9. In all methods, we reduced 20,531 columns to 40 columns. While this reduction might not have been optimal for all methods, it allows us to compare the preservation of distances after the same amount of reduction. The results are dramatic. Clearly, the column sketch outperforms the other methods. Incidentally, we omitted manifold learning methods because they do not scale practically to this sized data matrix (Tang et al., 2016).

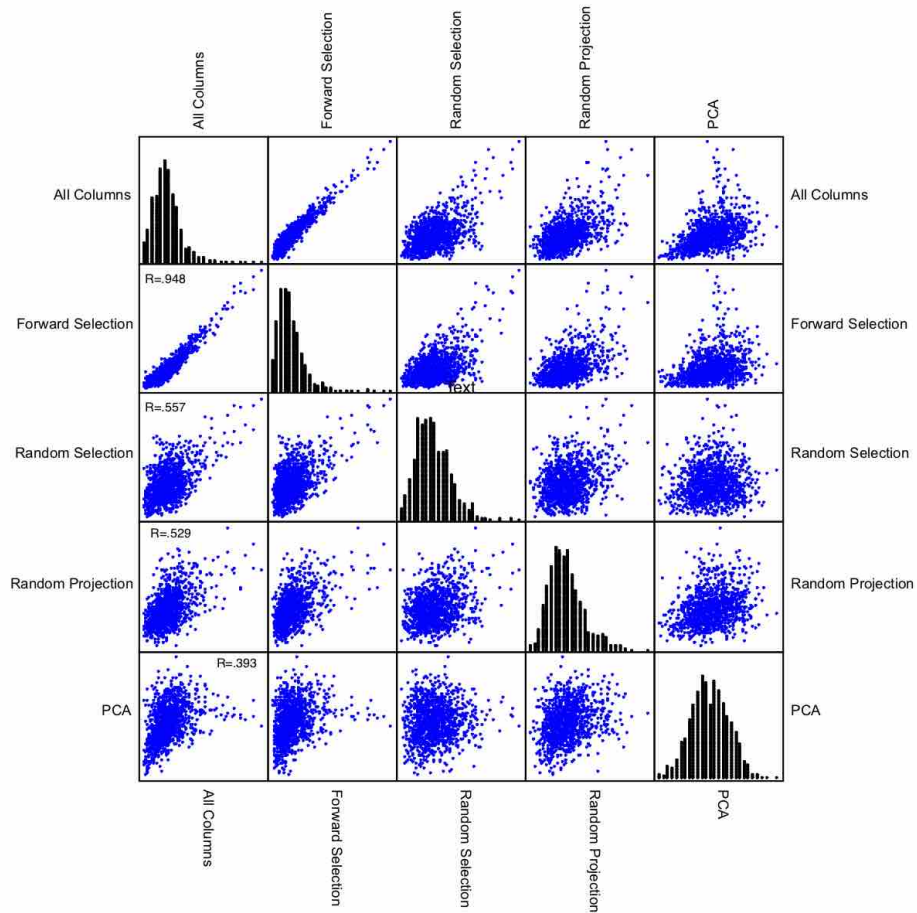


Figure 4: Comparison of column reducing algorithms using the gene expression dataset. The points in the plots represent all pairwise distances between points in higher-dimensional space (20,531 dimensions) and pairwise distances between the same points in projected space (40 dimensions). Forward selection column sketching is the only algorithm in this collection that substantially preserves relative distances among points.

**Accuracy of Sketching** A simple test of the column reducing algorithm is to compute two analyses of the same data – one on the full dataset and the other on the column-sketched dataset. Figure 5 shows two multidimensional scalings. The upper panel shows the scaling of 77 cereals from a kaggle dataset (<https://www.kaggle.com/crawford/80-cereals>). There are 13 continuous variables represented by the columns (calories, protein, fat, sodium, fiber, carbo, sugars, potassium,

vitamins, shelf, weight, cups, rating). We computed Euclidean distances among the cereals based on all 13 columns and then did an *MDS* on the resulting distance matrix. The cereals are colored blue in this coordinate plot.

The lower panel, in black, shows the scaling of the same cereals using seven columns selected by the column sketch algorithm (calories, sodium, fiber, sugars, potassium, vitamins, shelf). The Frobenius correlation between the row distances in the full dataset and in the sketch dataset is 0.98. While there are some differences in detail, the result of the sketch algorithm is visibly close to the result based on all the variables. This is due to the 0.98 correlation between output distances of sketching and all columns. When this correlation is high, we can expect the results of distance preserving algorithms (like *MDS*) to be similar in both cases. This will not be necessarily true if we use analytic visualization methods that do not preserve distances (such as principal components, *tSNE*, or *UMAP*).



Figure 5: Comparison of analyses based on the column sketch algorithm (lower panel) and all columns (upper panel) using a cereals dataset from kaggle.

**Using Matrix Column Sketching as a Feature Selector in Supervised Learning.** Although matrix sketching is not designed to serve as a feature selection method for supervised learning, we might want to see if it could help in such an application. (Feature selection in *supervised learning* leverages the predictive ability of each predictor in a training set and discards ineffective predictors; matrix sketching is an *unsupervised* algorithm that gives us no access to a dependent variable.) Figure 6 shows the results of using a lightGBM model (<https://lightgbm.readthedocs.io/en/latest/>) on the Madelon dataset (<http://archive.ics.uci.edu/ml/datasets/madelon>). The left panel shows the Receiver Operating Characteristic (ROC) curve for the model based on all 500 columns of the original dataset. The right panel shows the ROC result for 50 columns selected by matrix sketching. Despite the fact that our sketching algorithm knew nothing about the predicted variable, it derived a subset of columns that were practically useful in making a prediction.

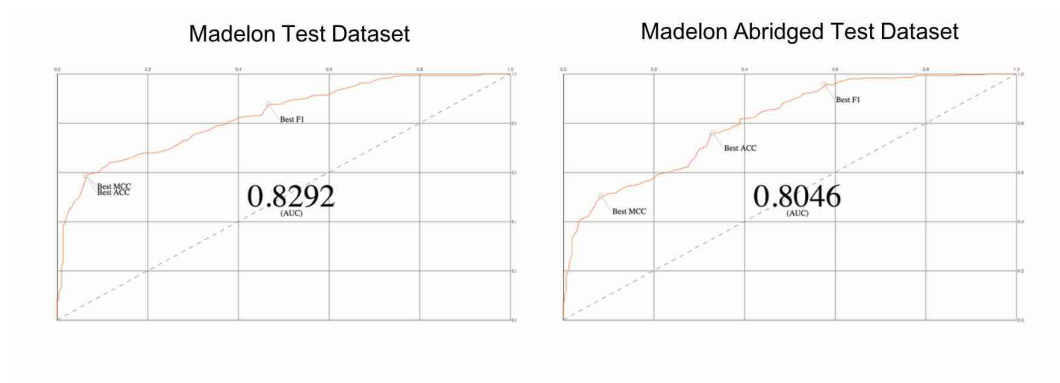


Figure 6: ROC plot (left) based on Madelon dataset (500 columns) and ROC plot (right) based on sketched Madelon dataset (50 columns)

### 3.3 Data Visualization

This section presents several multivariate visualizations that are particularly suited to our matrix sketching algorithm on rows and columns of data matrix.

### 3.3.1 Biplots

**Visualization via Biplots** Figure 7 shows a biplot (Gabriel, 1971) of the Madelon training dataset. We reduced 2000 rows to 1000 and 500 columns to 20.

This biplot represents principal component loadings with vectors (red) and scores with points (blue) – all in the same frame. The biplot in the left panel obscures most of the variation in cases and variables. The biplot in the right panel shows the 20 vectors representing the column variables. The canonical correlation between the coordinates of the vectors in the right plot with the coordinates of the corresponding vectors in the left plot is 0.89. This indicates that the right plot is accurately representing the relevant loadings in the principal components of the full dataset. In addition, the sketch plot spans the full 2D space the way the full-data plot does. It is not a seriously biased representation.

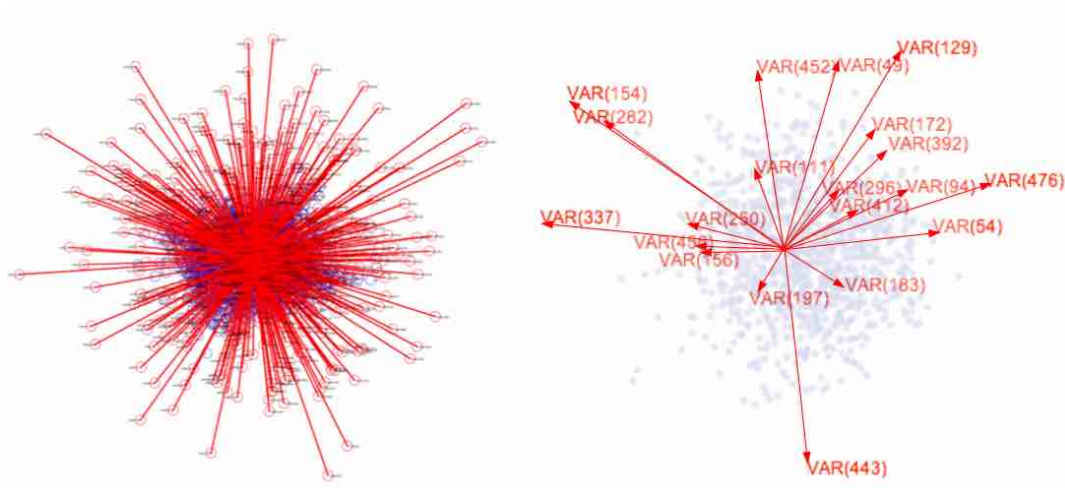


Figure 7: Full Madelon dataset biplot (left) and matrix sketched dataset biplot (right).

### 3.3.2 Parallel Coordinates

Parallel Coordinates, in various forms, are one of the most popular multidimensional visual analytic methods for big data (Inselberg, 2009; Zhang and Huang, 2016; Johansson et al., 2005). Their well-known weakness is visual clutter, caused both by many cases and many variables. Obvious remedies for this problem include the use of ker-

nels, profile aggregation, and sorting of variables to reduce crossings. Our sketching algorithm on rows and columns makes all these remedies easier to realize, especially with limited computational resources.

Figure 8 shows parallel coordinates using our sketching algorithm on rows and columns on a popular dataset comprising delays in air traffic performance ([https://www.transtats.bts.gov/OT\\_Delay/OT\\_DelayCause1.asp](https://www.transtats.bts.gov/OT_Delay/OT_DelayCause1.asp)). A  $k$ -means cluster analysis is used to color the display, which clearly reveals two different clusters (Caliński and Harabasz, 1974) on the performance variables.

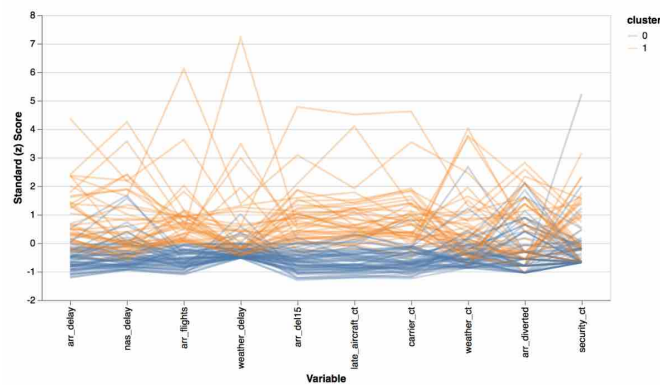


Figure 8: Parallel Coordinates plot of 1762 rows reduced to 99 and 22 columns reduced to 10 columns

### 3.3.3 Heatmaps

Cluster heatmaps involve joint reorderings of the rows and columns of a data matrix using hierarchical clustering (Wilkinson and Friendly, 2009). They are impractical for big data for two reasons. First, display resolution prevents rendering of cells in large heatmaps, even when cells are depicted in single pixels. Second, the number of rows and/or columns in big data matrices exceeds the computational efficiency of hierarchical clustering. Matrix sketching is suited as a remedy for these problems.

Figure 9 shows a cluster heatmap of gene expression data using matrix sketching. The data are from Weinstein et al. (2013), see also Khomtchouk et al. (2017). We reduced 801 rows and 20,531 columns to 47 rows and 40 columns. The display indicates

joint clusters (particularly in the lower left) that might be fruitful for further analysis. We cannot compare this heatmap to others on this dataset because we could not find any heatmap programs that could handle a dataset this size.

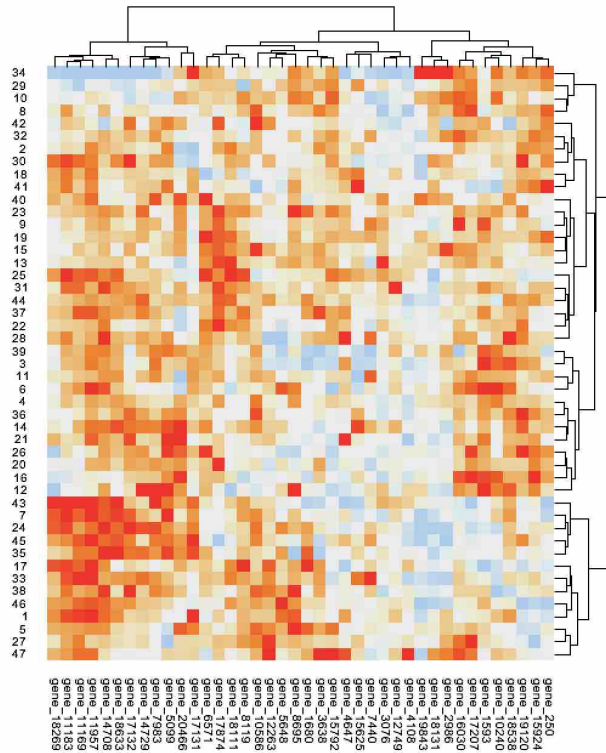


Figure 9: Heatmap of matrix-sketched gene expression data.

### 3.3.4 Scatterplot Matrices

Figure 10 shows a scatterplot matrix on sketched columns of the Madelon dataset. There are two interesting aspects of these plots. First, the sketched columns reveal anomalous artificial structures embedded in this dataset. In particular, the two straight-line relationships between columns clearly stand out against the other patterns. These are the only anomalous ones of this kind in the whole dataset. Sketching is not an anomaly detector, but when embedded among relatively homogeneous distributions, anomalous relations are likely to be exposed. Columns on which there are outliers, for example, will have more leverage in the distance correlation calculations. Second, the



two SPLOMs are remarkably similar.

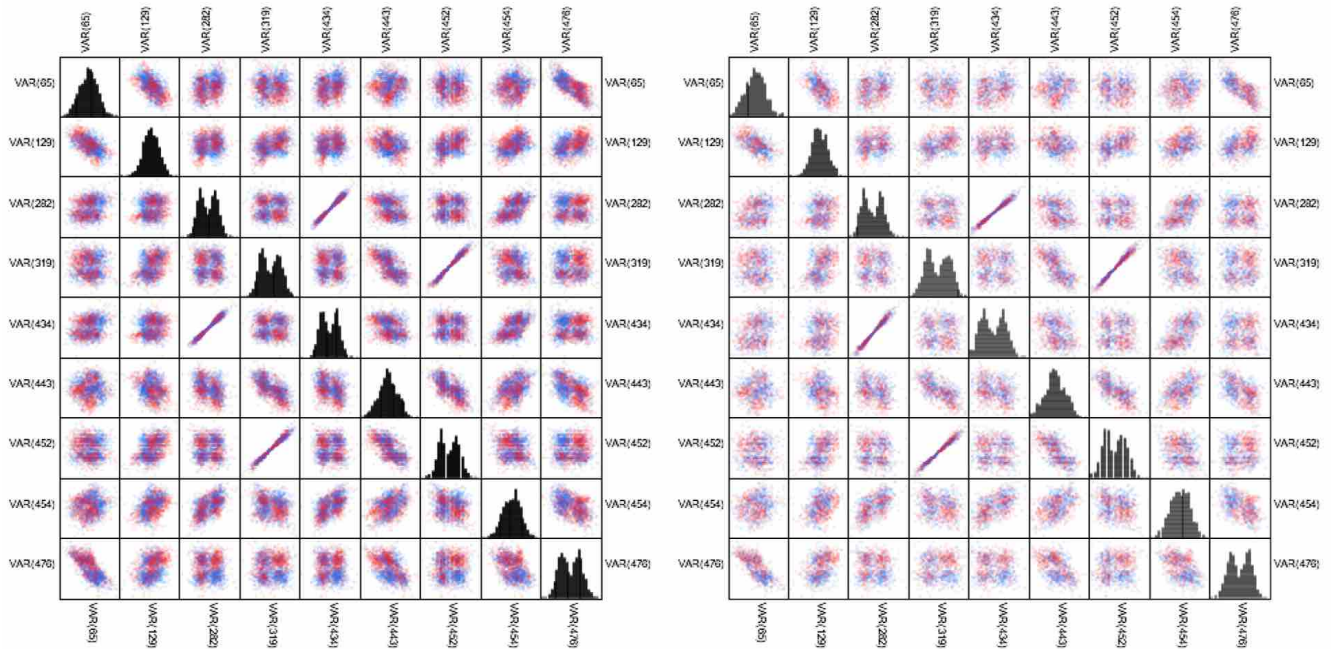


Figure 10: SPLOM on 2000 Madelon rows (left) and 1000 (right), 500 columns reduced to 10. The tenth variable (CLASS) is used to color the scatterplots.

### 3.3.5 Categorical Variables

To incorporate categorical variables (string columns), we need to convert categories to numerical values. Correspondence Analysis (CA) (Greenacre, 1984; Greenacre and Blasius, 2006) was designed for this purpose. We begin by representing a categorical variable with a set of dummy codes, one code (1 or 0) for each category. These codes comprise a matrix of 1's and 0's with as many columns as there are categories on that variable. We then compute a principal components decomposition of the covariance matrix of the dummy codes. This analysis is done separately for each of  $k$  categorical variables in a dataset. CA scores on the rows are computed on each categorical variable by multiplying the dummy codes on that row's variable times the eigenvectors of the decomposition for that variable. Computing the decomposition separately for each

categorical variable is equivalent to doing a multiple correspondence analysis separately for each variable instead of pooling all the categorical variable dummy codes into one matrix. This application of CA to deal with visualization of nominal data was first presented in (Rosario et al., 2004).

## 4 Conclusion

In a landmark paper relatively unknown to many computer scientists and statisticians today, Amos Tversky discussed the use of real vector spaces in data science (Tversky., 1977). At the time of the paper, psychologists were enthusiastic about the possibility of using multidimensional scaling (*MDS*) to derive a cognitive map (points in a metric space) from judgments of the similarities between objects. Tversky demonstrated that some types of data are inappropriate for methods that depend on metric axioms. A simple example is the triad of statements most observers would agree with:

- Miami is similar to Havana
- Havana is similar to Moscow
- But Miami is not similar to Moscow

Tversky argued against the indiscriminate use of metric space models in psychology, but there is perhaps a wider range of indiscriminate usage of nonlinear manifold models in machine learning and visualization today. Users of these methods may assume that they are appropriate for any numerical data.

A corollary of Tversky's observation, in the context of today's multidimensional visualization practices, might be our point in the Related Work section that visualizations that violate metric axioms can be harmful, leading viewers to misinterpret similarities between objects. Judging dissimilar points as similar or similar points as dissimilar can lead to false conclusions. Today's popular multidimensional visualization algorithms are not intrinsically flawed; their flaws lie in their indiscriminate uses that do not take into account the assumptions underlying them.

In addition to the primary motivation for this research (distance-preservation un-

der projections), there is a significant concomitant benefit. It involves reification of composites. As Drineas et al. (2008) point out,

Although the truncated *SVD* is widely used, the vectors  $u^i$  and  $v^i$  themselves may lack any meaning in terms of the field from which the data are drawn. For example, the eigenvector

$$[(1/2)age - (1/\sqrt{2})height + (1/2)income],$$

being one of the significant uncorrelated “factors” or “features” from a dataset of people’s features, is not particularly informative or meaningful. This fact should not be surprising. After all, the singular vectors are mathematical abstractions that can be calculated for any data matrix. They are not “things” with a “physical” reality.

Nevertheless, data analysts often fall prey to a temptation for reification, i.e., for assigning a physical meaning or interpretation to all large singular components.

Mahoney and Drineas explain axis-parallel representation as a strength of the *CUR* decomposition. We agree. While our algorithm is fundamentally different from theirs, it shares interpretive advantages with *CUR*.

We do not propose that our sketching algorithm on rows and columns replace other methods for handling big data problems. Each method has its own advantages. Our algorithm on rows and columns has several, each designed to facilitate visual analysis of large datasets. First, it returns a subset of a given matrix, not a set of additive composites. This facilitates brushing and linking to real data values rather than to composites. Second, our algorithm is more scalable than other projection methods, especially iterative ones like manifold learning or projection pursuit. And, finally, our algorithm is distance-preserving so that the resulting low-dimensional visualizations are less likely to violate the metric axioms when we use sketching inside the visualization flow running from data to perceived structures, patterns, and relationships.

## SUPPLEMENTAL MATERIALS

# A Error Bounds and Distance Preserving Properties

## A.1 Row Algorithm Error Bound

For the row (Leader) algorithm, the error for exemplar-to-exemplar distances is zero because the exemplars are original data points.

For member-to-member, the worst case error for a single pair is  $2r$ , where each point is at the furthest boundary of the ball in which it is a member relative to the other point in the pair, which is at the furthest point in its own ball. Since the estimate of the distance between the two points is based on the respective exemplars,  $2r$  is the worst possible error in this case.

For example, in Figure 11, the true distance between points  $x$  and  $y$  is  $r + d + r$ . But in the reduced dataset, distance between points  $x$  and  $y$  will be the inter-exemplar distance  $d$ . So the error between the pairwise distance of  $x, y$  in the original and reduced dataset is  $2r$ .

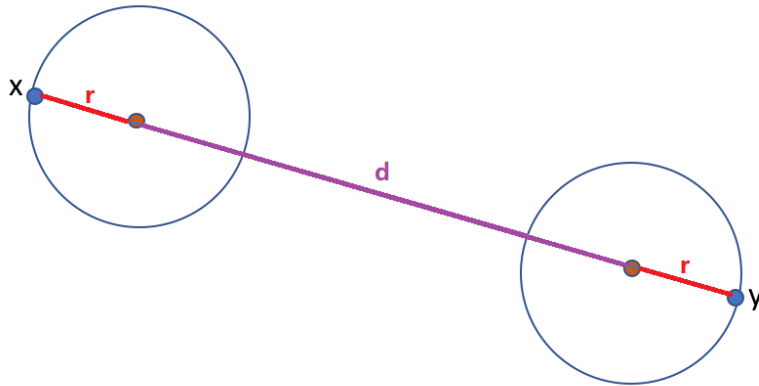


Figure 11: Distances between exemplars and extremes in 2 dimension.

Pairwise distances are the only concern in the row sketching algorithm. Since we fix the radius  $r$  of each exemplar, we need to know the minimal number of exemplar we needed.  $r$ -covering number for the dataset represented by the  $n \times p$  data matrix  $X$ . If we know the distribution of the dataset, we could integrate this over all points to get the worst case overall error and expected error.

Practically, we usually normalize each column of the  $n \times p$  data matrix  $X$  such that each entry in  $X$  is in  $[0, 1]$ , therefore each squared pairwise distance  $d(X(i,:), X(j,:))^2$  is in  $[0, p]$ . Instead of removing rows from  $X$  in row algorithm, we simply replace the rows of data points with the row of corresponding exemplar to obtain reduced  $n \times p$  matrix  $X_{(R)}$ . Only the non-repetitive rows represent data points.

$$\begin{aligned} d(X(i,:), X(j,:))^2 - d(X_{(R)}(i,:), X_{(R)}(j,:))^2 &= [d(X(i,:), X(j,:)) - d(X_{(R)}(i,:), X_{(R)}(j,:))] \cdot \\ &\quad [d(X(i,:), X(j,:)) + d(X_{(R)}(i,:), X_{(R)}(j,:))] \\ &\leq 2r \cdot 2\sqrt{p} \\ &\leq 4\sqrt{pr} \end{aligned}$$

**Theorem 1.** Consider the normalized data matrix  $X$ . We use the notation  $X_{ij}$  to denote the  $(i, j)$ -th entry;  $X(i, :)$  to denote the  $i$ -th row;  $X(:, j)$  to denote the  $j$ -th column of the  $m \times p$  data matrix  $X$ , and we use subscript  $X_{(R)}$  to denote the distance matrix after row reduction. Then

$$\max_{i,j} \left| d(X(i,:), X(j,:))^2 - d(X_{(R)}(i,:), X_{(R)}(j,:))^2 \right| \leq 4\sqrt{pr},$$

Note that the distances between exemplars are unchanged and the differences between these pairs are zero. Suppose there are  $K(r) \leq n$  exemplars, then there are  $(n - K(r)) \cdot (n - K(r) - 1)$  pairs of non-exemplars, and  $K(r)(n - K(r))$  exemplar-non-exemplar pairs. The overall error can be described by

$$\begin{aligned} &\sum_{i,j} \left| d(X(i,:), X(j,:))^2 - d(X_{(R)}(i,:), X_{(R)}(j,:))^2 \right| \\ &\leq 4\sqrt{pr} \cdot [(n - K(r)) \cdot (n - K(r) - 1) + K(r)(n - K(r))] \cdot \\ &= 4\sqrt{pr} \cdot (n - K(r)) \cdot (n - 1) \end{aligned}$$

Although  $K(r)$  is non-increasing in  $r$  (i.e.  $n - K(r)$  is non-decreasing), we do not

have an explicit expression of the quantity  $K(r)$ . However, we can sometimes have a probabilistic estimate when the distributional properties of  $X$  is known.

Empirically, for a fixed  $n$ , if  $r$  is small enough, then the row algorithm produces negligible error for all points and the overall error depends mostly on the column algorithm. For which we will discuss in length below.

## A.2 Column Algorithm Error Bound

### A.2.1 Column Sketching with Frobenius coefficient

When we use the Frobenius coefficient to measure the similarity between squared distance matrices, an error bound for the column algorithm involving  $\varepsilon$  could be derived as below.

The Frobenius matrix inner product between two  $m \times p$  matrices  $A, B$  is defined as  $\langle A, B \rangle := \text{tr}(A^T B)$  for the space consisting of all  $m \times p$  matrices is an inner space, denoted as  $\mathbb{R}^{m \times p}$ . With this notion of inner product and its induced Frobenius norm  $\|A\|_F := \text{tr}(A^T A)$ , we can define the cosine between two matrices  $A, B \in \mathbb{R}^{m \times p}$  as  $\cos(A, B) := \frac{\langle A, B \rangle}{\sqrt{\langle A, A \rangle \cdot \langle B, B \rangle}}$ .

We use the notation  $X_{ij}$  to denote the  $(i, j)$ -th entry;  $X(i, :)$  to denote the  $i$ -th row;  $X(:, j)$  to denote the  $j$ -th column of the  $m \times p$  data matrix  $X$ , and we use subscript  $D_{(k)}$  to denote the distance matrix in the  $k$ -th loop.

The column algorithm starts with a *squared distance matrix*  $D_{(0)} = 0 \in \mathbb{R}^{m^2 \times m^2}$  (we assume a full distance matrix instead of an  $\frac{m(m-1)}{2}$  array) with all entries being zero. We can compute  $D_{(j)} = \text{dist}(X(:, j))$ ,  $j = 1, \dots, p$  to be squared distance matrices for the  $j$ -th column of the data matrix  $X$ . This indexing shall not be confused with our subscript convention above.

Then, we choose one column from the data matrix  $X$  such that the  $\max_{j=1, \dots, p} \cos(D_X, D_{(j)})$  is attained by using the squared distance matrix of this column. In the space  $\mathbb{R}^{m^2 \times m^2}$ , this choice is equivalent to choosing from “vectors”  $D_{(1)}, \dots, D_{(p)}$  such that the cosine is maximized. Geometrically, we choose one vector in the space  $\mathbb{R}^{m^2 \times m^2}$  which has the smallest angle against  $D_X$ . Then we update the  $D_{(0)}$  to be  $D_{(1)}$ . By the

Pythagorean theorem, the  $(i, j)$ -th entry of  $D_X$  is  $\|X(i, :) - X(j, :)\|_2^2$ , which can be decomposed into  $\sum_{k=1, \dots, p} |X_{ik} - X_{jk}|^2 = \sum_{k=1, \dots, p} D(k)_{ij}$  due to orthogonality. Examine each entry in both distance matrices, we have

$$D_X = \sum_{k=1, \dots, p} D(k),$$

which explains why the  $D_{(0)}, D_{(1)}, \dots$  are updated additively in each loop.

In short, we start from a zero distance matrix  $D_{(0)}$  and subsequently choose from  $D(1), \dots, D(p)$  to approach the direction of  $D_X$  until either we reach  $D_X = \sum_{k=1, \dots, p} D(k)$  or the  $D_{(C)}$  has a sufficiently small angle (measured by threshold  $\epsilon$ ) to  $D_X$ .

**Example 1.** (Co-planar example) Consider a concrete example of  $3 \times 3$  matrix  $X = \begin{pmatrix} 0 & 1 & 2 \\ 0 & 4 & 5 \\ 0 & 6 & 9 \end{pmatrix}$ , which represents 3 points  $(0, 1, 2)^T, (0, 4, 5)^T, (0, 6, 9)^T$  in  $\mathbb{R}^3$ .

In the column algorithm we have initialized  $D_{(0)} = \begin{pmatrix} 0 & 0 & 0 \\ 0 & 0 & 0 \\ 0 & 0 & 0 \end{pmatrix}$ , and the distance matrix for the full dataset is  $D_X = \text{dist}(X) = \begin{pmatrix} 0 & 18 & 50 \\ 18 & 0 & 8 \\ 50 & 8 & 0 \end{pmatrix}$ .

For each of 3 columns we compute

$$D(1) = \text{dist}(X(:, 1)) = \begin{pmatrix} 0 & 0 & 0 \\ 0 & 0 & 0 \\ 0 & 0 & 0 \end{pmatrix}, \quad \cos(D_X, D(1)) = 0,$$

$$D(2) = \text{dist}(X(:, 2)) = \begin{pmatrix} 0 & 9 & 25 \\ 9 & 0 & 4 \\ 25 & 4 & 0 \end{pmatrix}, \quad \cos(D_X, D(2)) = \frac{2888}{\sqrt{5776 \times 1444}} = 1,$$

$$D(3) = \text{dist}(X(:,3)) = \begin{pmatrix} 0 & 9 & 49 \\ 9 & 0 & 16 \\ 49 & 16 & 0 \end{pmatrix}, \quad \cos(D_X, D(3)) = \frac{5480}{\sqrt{5776 \times 5476}} \approx 0.97,$$

(also note that  $D_X = 2 \cdot D(2)$ ).

In the first loop, since the distance matrix  $D(2)$  has the largest cosine (i.e., smallest angle) to  $D_X$ , we select the second column in the first loop and update

$$D_{(1)} = D_{(0)} + D(2) = \begin{pmatrix} 0 & 9 & 25 \\ 9 & 0 & 4 \\ 25 & 4 & 0 \end{pmatrix}.$$

Before the second loop, we can compute that  $\cos(D_X, D_{(1)}) = \frac{8664}{\sqrt{5776 \times 12996}} = 1 > 0.95$  and this stops the column algorithm.

The column reduced matrix will be  $X_{\text{col reduced}} = X_{(1)} = \begin{pmatrix} 1 \\ 4 \\ 6 \end{pmatrix}$  with the only retained column being the second column in the original matrix.

$$\text{The distance matrix of the reduced matrix is } \begin{pmatrix} 0 & 9 & 25 \\ 9 & 0 & 4 \\ 25 & 4 & 0 \end{pmatrix}.$$

This dataset is special in the sense that these 3 points are in fact living in y-z plane. Intuitively, we can drop the first column (x-axis in  $\mathbb{R}^3$ ) without disturbing pairwise distances. However, we also drop the third column, because all we care in the column algorithm with Frobenius coefficient is the direction of  $D_X$ , not even its modulus.

### A.2.2 Error Bound

Generally speaking, suppose we have chosen an  $m \times p$  data matrix  $X$  and a threshold  $\varepsilon \in (0, 1]$ , and the column algorithm stops after  $N \leq p$  steps.



**Step 1. Geometric distance between  $D_X, D_{(C)}$ .** We have stated in the sub-section and example above that the Frobenius coefficient or the cosine has a natural geometric interpretation. On one hand, we can assert that  $\cos(D_X, D_{(C)}) \geq \varepsilon$  and subsequently  $\sin(D_X, D_{(C)}) \leq \sqrt{1 - \varepsilon^2}$  since  $\sin^2 \theta + \cos^2 \theta = 1$ . The difference between  $D_X, D_{(C)}$  can be written as  $\|D_X - D_{(C)}\|_F$ , by trigonometric geometry, we know that

$$\|D_X - D_{(C)}\|_F \leq \max(\|D_X\|_F, \|D_{(C)}\|_F) \cdot \sin(D_X, D_{(C)}) \leq \max(\|D_X\|_F, \|D_{(C)}\|_F) \cdot \sqrt{1 - \varepsilon^2}.$$

On the other hand, we know that  $\|A\|_F = \sqrt{\sum_{i=1}^m \sum_{j=1}^n |a_{ij}|^2} \geq \max_{i,j} |a_{ij}| =: \|A\|_{\max}$  for a matrix  $A = \llbracket a_{ij} \rrbracket$  (See, e.g., Horn and Johnson (2012)). Therefore,

$$\|D_X - D_{(C)}\|_{\max} \leq \max(\|D_X\|_F, \|D_{(C)}\|_F) \cdot \sqrt{1 - \varepsilon^2}.$$

**Step 2.  $D_X, D_{(C)}$  as (normalized) squared distance matrices.** But the  $(i, j)$ -th entry in  $D_X$  is the pairwise squared distance  $d(X(i, :), X(j, :))^2$  with Euclidean distance  $d$ , and the  $(i, j)$ -th entry in  $D_{(C)}$  is the pairwise distance  $d(X_{(C)}(i, :), X_{(C)}(j, :))$ , we know that

$$\max_{i,j} \left| d(X(i, :), X(j, :))^2 - d(X_{(C)}(i, :), X_{(C)}(j, :))^2 \right| \leq \max(\|D_X\|_F, \|D_{(C)}\|_F) \cdot \sqrt{1 - \varepsilon^2},$$

The left hand side of this inequality is the maximal difference between pairwise squared distances calculated in the original and column reduced dataset.

However, in practice we usually normalize each column of  $X$  such that each entry in  $X$  is in  $[0, 1]$ . Note that  $D_{(C)}$  is a submatrix of  $D_X$  and each entry of  $D_X, D_{(C)}$  are inside  $[0, p]$ . By definition,  $\|A\|_F = \sqrt{\text{tr}(A^T A)} = \sqrt{\sum_{i=1}^m \sum_{j=1}^n |a_{ij}|^2}$  we have

$$\max(\|D_X\|_F, \|D_{(C)}\|_F) \leq \sqrt{\sum_{i=1}^m \sum_{j=1}^m p^2} = mp, \quad (4)$$

since each entry of both distance matrices are bounded in a unit hyper-cube with dimension at most  $p$ .

**Theorem 2.** Given an  $m \times p$  data matrix  $X$ , we supply it as the input of column algorithm with threshold  $\varepsilon \in (0, 1]$ . We denote the output matrix of column algorithm as  $X_{(C)}$ , where  $0 \leq N \leq p$  is the number of loops until stopping. The notation  $D_X = \llbracket d(X(i,:), X(j,:)) \rrbracket$  and  $D_{(C)} = \llbracket d(X_{(C)}(i,:), X_{(C)}(j,:)) \rrbracket$ . Then,

$$\max_{i,j} \left| d(X(i,:), X(j,:))^2 - d(X_{(C)}(i,:), X_{(C)}(j,:))^2 \right| \leq C_1 \cdot \sqrt{1 - \varepsilon^2},$$

where  $C_1$  is a positive constant s.t.  $C_1 \geq mp$ .

Since both  $D_X, D_{(C)}$  are symmetric interval matrices (Hladík et al., 2010) with entries in  $[0, p]$  with column normalization, a sharper constant  $C$  could be arithmetically obtained. Let's try this error bound with the co-planar example again.

**Example 2.** (Normalized co-planar example) Consider again the example of  $3 \times 3$

matrix  $X = \begin{pmatrix} 0 & 1 & 2 \\ 0 & 4 & 5 \\ 0 & 6 & 9 \end{pmatrix}$ , which represents 3 points  $(0, 1, 2)^T, (0, 4, 5)^T, (0, 6, 9)^T$  in

$\mathbb{R}^3$ . Let's normalize columns of this data matrix into  $\tilde{X} = \begin{pmatrix} 0 & 1/11 & 2/16 \\ 0 & 4/11 & 5/16 \\ 0 & 6/11 & 9/16 \end{pmatrix}$

In the column algorithm we have initialized  $D_{(0)} = \begin{pmatrix} 0 & 0 & 0 \\ 0 & 0 & 0 \\ 0 & 0 & 0 \end{pmatrix}$ , and the distance

matrix for the full dataset is  $D_X = \text{dist}(X) = \begin{pmatrix} 0 & 0.11 & 0.40 \\ 0.11 & 0 & 0.10 \\ 0.40 & 0.10 & 0 \end{pmatrix}$  (rounded-off to

the second decimal).

For each of 3 columns we compute

$$D(1) = \text{dist}(X(:,1)) = \begin{pmatrix} 0 & 0 & 0 \\ 0 & 0 & 0 \\ 0 & 0 & 0 \end{pmatrix}, \quad \cos(D_X, D(1)) = 0.00,$$

$$D(2) = \text{dist}(X(:,2)) = \begin{pmatrix} 0 & 0.07 & 0.21 \\ 0.07 & 0 & 0.03 \\ 0.21 & 0.03 & 0 \end{pmatrix}, \quad \cos(D_X, D(2)) \approx 0.994101,$$

$$D(3) = \text{dist}(X(:,3)) = \begin{pmatrix} 0 & 0.04 & 0.19 \\ 0.04 & 0 & 0.06 \\ 0.19 & 0.06 & 0 \end{pmatrix}, \quad \cos(D_X, D(3)) \approx 0.9930334,$$

In the first loop, since the distance matrix  $D(2)$  has the largest cosine (i.e., smallest angle) to  $D_X$ , we select the second column in the first loop and update

$$D_{(1)} = D_{(0)} + D(2) = \begin{pmatrix} 0 & 0.07 & 0.21 \\ 0.07 & 0 & 0.03 \\ 0.21 & 0.03 & 0 \end{pmatrix}.$$

Before the second loop, we can compute that  $\cos(D_X, D_{(1)}) = 1.00 > 0.95$  and this stops the column algorithm with only  $X(:,1)$  retained.

The error bound obtain with  $C = m\sqrt{p}$  is  $m\sqrt{p} \cdot \sqrt{1 - \epsilon^2} = 3 \cdot 3 \cdot \sqrt{1 - 0.95^2} \approx 2.810249$ , and the difference

$$\max_{i,j} \left| d(X(i,:), X(j,:))^2 - d(X_{(1)}(i,:), X_{(1)}(j,:))^2 \right| \approx 0.19140625 \quad (5)$$

is attained for  $i = 3, j = 1$ , which is clearly bounded by 2.810249.

The error bound also serves as a theoretical support for the claimed “distance-preserving property” of column sketching, since the difference between  $D_X, D_{(C)}$  is essentially bounded by a quantity only depends on  $m, p$  and threshold  $\varepsilon$ .

Interestingly, in this example, even if we choose  $\varepsilon = 0.99$ , the result is still holds with one loop, but with a tighter bound 0.733. But if we set the  $\varepsilon = 0.999$  then the error bound becomes 0.4023916. But this is not a flaw of our result, since with  $\varepsilon = 0.999$ , the column algorithm does not stop until second loop. After that, it includes both the second and the third column, for which we can clearly see  $D_{(2)} = D_{(0)} + D(2) + D(3)$  and  $\cos(D_X, D_{(2)}) = 1 > 0.999, D_{(2)} = D_X$ . Since the constant  $C$  is generally not sharp, there is not a deterministic relation between the choice of threshold  $\varepsilon$  and maximal error between squared distances. However, if we want to control error bound, then the theorem will help us choosing  $\varepsilon$  given an  $m \times p$  data matrix  $X$ .

## References

- P. K. Agarwal, S. Har-Peled, and K. R. Varadarajan. Geometric approximation via coresets. *Combinatorial and computational geometry*, 52:1–30, 2005.
- S.M. Ali, N. Gupta, G.K. Nayak, and R.K. Lenka. Big data visualization: Tools and challenges. In *2016 2nd International Conference on Contemporary Computing and Informatics (IC3I)*. IEEE, 2016.
- D. Asimov. The grand tour: A tool for viewing multidimensional data. *SIAM Journal on Scientific and Statistical Computing*, 6:128–143, 1985.
- A. Batch and Niklas Elmqvist. The interactive visualization gap in initial exploratory data analysis. *IEEE Transactions on Visualization and Computer Graphics*, 24:278–287, 2017.
- M. Belkin and P. Niyogi. Laplacian eigenmaps for dimensionality reduction and data representation. *Neural Computation*, 15:1373–1396, 2003.
- T. Caliński and J. Harabasz. A dendrite method for cluster analysis. *Communications in Statistics-Simulation and Computation*, 3(1):1–27, 1974.
- D. B. Carr, R. J. Littlefield, W. L. Nicholson, and J. S. Littlefield. Scatterplot matrix techniques for large n. *Journal of the American Statistical Association*, 82:424–436, 1987.
- D.B. Carr, R. Kahn, K. Sahr, and A. R. Olsen. ISEA discrete global grids. *Statistical Computing & Graphics Newsletter*, 8:31–39, 1997.
- M. Cavallo and C. Demiralp. A visual interaction framework for dimensionality reduction based data exploration. In *Extended Abstracts of the 2018 CHI Conference on Human Factors in Computing Systems*, CHI EA '18, New York, NY, USA, 2018. Association for Computing Machinery.

- C. H. Cheng, A. W. Fu, and Y. Zhang. Entropy-based subspace clustering for mining numerical data. In *KDD '99*, 1999.
- G. Cormode and A. McGregor. Approximation algorithms for clustering uncertain data. *PODS '08*, pages 191–200, 2008.
- C. Ding and X. He. K-means clustering via principal component analysis. In *ICML '04: Proceedings of the twenty-first international conference on Machine learning*, pages 6–15. IEEE, 2004a.
- C. Ding and X. He. Cluster structure of k-means clustering via principal component analysis. In *PAKDD 2004: Advances in Knowledge Discovery and Data Mining*, pages 414–418. Springer, 2004b.
- P. Drineas, M. W. Mahoney, and S. Muthukrishnan. Relative-error *cur* matrix decompositions. *SIAM Journal on Matrix Analysis and Applications*, 30:844–881, 2008.
- W. DuMouchel. Data squashing: Constructing summary data sets. In J. Abello, P.M. Pardalos, and M.G.C. Resende, editors, *Handbook of Massive Data Sets: Massive Computing*, pages 579–591. Springer, Boston, 2002.
- W. DuMouchel, C. Volinsky, T. Johnson, C. Cortes, and D. Pregibon. Combining automated analysis and visualization techniques for effective exploration of high-dimensional data. In *Proceedings of the Fifth ACM Conference on Knowledge Discovery and Data Mining*, pages 6–15. IEEE, 1999.
- J.G. Dy and C.E. Brodley. Feature selection for unsupervised learning. *Journal of Machine Learning Research*, 5:845–889, 2004.
- J. Fekete and C. Plaisant. Interactive information visualization of a million items. *IEEE Symposium on Information Visualization, 2002. INFOVIS 2002.*, pages 117–124, 2002.
- J.H. Friedman and J.J. Meulman. Clustering objects on subsets of attributes. *Journal of the Royal Statistical Society*, 66:815–849, 2004.

- K.R. Gabriel. The biplot graphical display of matrices with application to principal component analysis. *Biometrika*, 58:453–467, 1971.
- M. Greenacre. *Theory and Applications of Correspondence Analysis*. Academic Press, 1984.
- M. Greenacre and J. Blasius. *Multiple Correspondence Analysis and Related Methods*. Chapman & Hall/CRC, 2006.
- I. Guyon, S. Gunn, M. Nikravesh, and L. A. Zadeh. *Feature Extraction: Foundations and Applications (Studies in Fuzziness and Soft Computing)*. Springer-Verlag, Berlin, Heidelberg, 2006.
- N. Halko, P.G. Martinsson, and J.A. Tropp. Finding structure with randomness: Probabilistic algorithms for constructing approximate matrix decompositions. *SIAM Review*, 53:217–288, 2011.
- J.A. Hartigan. *Clustering Algorithms*. John Wiley & Sons, New York, 1975.
- Milan Hladík, David Daney, and Elias Tsigaridas. Bounds on real eigenvalues and singular values of interval matrices. *SIAM Journal on Matrix Analysis and Applications*, 31(4):2116–2129, 2010.
- R. A. Horn and C. R. Johnson. *Matrix analysis*. Cambridge university press, 2012.
- H. Hotelling. Analysis of a complex of statistical variables into principal components. *Journal of Educational Psychology*, 24:417–441, 1933.
- W.W. Hsieh. Nonlinear principal component analysis. In Haupt S.E., Pasini A., and Marzban C., editors, *Artificial Intelligence Methods in the Environmental Sciences*, pages 173–190. Springer, Dordrecht, 2009.
- C. Hurley and R.W. Oldford. Pairwise display of high-dimensional information via eulerian tours and hamiltonian decompositions. *Journal of Computational and Graphical Statistics*, 2011. in press.

- A. Inselberg. *Parallel Coordinates: Visual Multidimensional Geometry and its Applications*. Springer-Verlag, New York, 2009.
- J. Johansson, P. Ljung, M. Jern, and M. Cooper. Revealing structure within clustered parallel coordinates displays. In *INFOVIS 2005: IEEE Symposium on Information Visualization*, pages 125–132. IEEE, 2005.
- W. B. Johnson and J. Lindenstrauss. Lipschitz mapping into Hilbert space. *Contemporary Mathematics*, 26:189–206, 1984.
- D.A. Keim. Designing pixel-oriented visualization techniques: theory and applications. *IEEE Transactions on Visualization and Computer Graphics*, 6:59–78, 2000.
- B. B. Khomtchouk, J. R. Hennessy, and C. Wahlestedt. shinyheatmap: Ultra fast low memory heatmap web interface for big data genomics. *PloS one*, 12(5):e0176334, 2017.
- J. A. Kimerling, K. Sahr, D. White, and L. Song. Comparing geometrical properties of global grids. *Cartography and Geographic Information Science*, 26:271–288, 1999.
- Y. Kosugi, J. Ikebe, N. Shitara, and K Takakura. Graphical presentation of multidimensional flow histogram using hexagonal segmentation. *Cytometry*, 7:291–294, 1986.
- J. Krause, A. Dasgupta, J.-D. Fekete, and E. Bertini. Seekaview: An intelligent dimensionality reduction strategy for navigating high-dimensional data spaces. In *2016 IEEE 6th Symposium on Large Data Analysis and Visualization (LDAV)*. IEEE, 2016.
- J. Kruskal. Multidimensional scaling by optimizing goodness of fit to a nonmetric hypo0. *Psychometrika*, 29(1):1–27, March 1964.
- E. Liberty. Simple and deterministic matrix sketching. In *Proceedings of the 19th ACM SIGKDD International Conference on Knowledge Discovery and Data Min-*



- ing, KDD '13, pages 581–588, New York, NY, USA, 2013. Association for Computing Machinery.
- S. Liu, D. Maljovec, B. Wang, P. Bremer, and V. Pascucci. Visualizing high-dimensional data: Advances in the past decade. *IEEE Transactions on Visualization and Computer Graphics*, 23(3):1249–1268, 2017.
- H. Luo, A. Patania, J. Kim, and M. Vejdemo-Johansson. Generalized penalty for circular coordinate representation. *arXiv:2006.02554*, pages 1–39, 2020.
- M. Mahajan, P. Nimbhorkar, and K. Varadarajan. The planar k-means problem is np-hard. In *International Workshop on Algorithms and Computation*, pages 274–285. Springer, 2009.
- L. McInnes, J. Healy, and J. Melville. UMAP: Uniform manifold approximation and projection for dimension reduction, 2018.
- C.A.L. Pahins, S.A. Stephens, C. Scheidegger, and J.L.D. Comba. Hashedcubes: Simple, low memory, real-time visual exploration of big data. *IEEE Transactions on Visualization and Computer Graphics*, 23:671–680, 2016.
- E. Paradis. Multidimensional scaling with very large datasets. *Journal of Computational and Graphical Statistics*, 27(4):935–939, 2018.
- H. Park, M. Jeon, and J.B. Rosen. Lower dimensional representation of text data based on centroids and least squares. *BIT Numerical Mathematics*, 43, 2003.
- K. Pearson. On lines and planes of closest fit to systems of points in space. *Philosophical Magazine*, 2:559–572, 1901.
- L. E. V. Peña, L. R. Mazahua, G. A. Hernández, B. A. O. Zepahua, S. G. P. Camarena, and I. M. Cano. Big data visualization: Review of techniques and datasets. In *2017 6th International Conference on Software Process Improvement (CIMPS)*, pages 1–9. IEEE, 2017.

- G. E. Rosario, E. A. Rundensteiner, D. C. Brown, M. O. Ward, and S. Huang. Mapping nominal values to numbers for effective visualization. *Information Visualization*, 3(2):80–95, June 2004. ISSN 1473-8716.
- P. Rousseeuw. Silhouettes: A graphical aid to the interpretation and validation of cluster analysis. *Journal of Computational and Applied Mathematics*, 20(1):53–65, November 1987.
- S. T. Roweis and L. K. Saul. Nonlinear dimensionality reduction by locally linear embedding. *Science*, 290:2323–2326, 2000.
- K. Sayood. *Introduction to Data Compression*. Morgan-Kaufmann, New York, 4th edition, 2012.
- R. N. Shepard. The analysis of proximities: Multidimensional scaling with an unknown distance function. I. *Psychometrika*, 27:125–139, 1962a.
- R. N. Shepard. The analysis of proximities: Multidimensional scaling with an unknown distance function. II. *Psychometrika*, 27:219–246, 1962b.
- R.N. Shepard and J.D. Carroll. Parametric representation of nonlinear data structures. In P.R. Krishnaiah, editor, *Multivariate Analysis*, pages 561–592. Academic Press, New York, 1966.
- G. W. Stewart and G. W. Stewart. Four algorithms for the the efficient computation of truncated pivoted qr approximations to a sparse matrix. *Numerische Mathematik*, 83:313–323, 1998.
- J. Tang, J. Liu, M. Zhang, and Q. Mei. Visualization large-scale and high-dimensional data. *CoRR*, 2016.
- A. Tatu, G. Albuquerque, M. Eisemann, P. Bak, H. Theisel, M. Magnor, and D. Keim. Automated analytical methods to support visual exploration of high-dimensional data. *IEEE Transactions on Visualization and Computer Graphics*, 17(5):584–597, 2011.

- J. B Tenenbaum, V. de Silva, and J. C Langford. A global geometric framework for nonlinear dimensionality reduction. *Science*, 290(5500):2319–2323, 2000.
- A. Tversky. Features of similarity. *Psychological Review*, 84:327–352, 1977.
- A. Unwin, M. Theus, and H. Hofmann. *Graphics of Large Datasets: Visualizing a Million*. Springer-Verlag, New York, 2007.
- L.J.P. van der Maaten and G.E. Hinton. Visualizing high-dimensional data using t-SNE. *Journal of Machine Learning Research*, 9:2579–2605, 2008.
- M. Wattenberg, F. Viégas, and I. Johnson. How to use t-sne effectively. *Distill*, 2016. doi: 10.23915/distill.00002.
- J. N. Weinstein, E. A Collisson, G. B. Mills, K. R. Mills Shaw, B. A. Ozenberger, K. Ellrott, I. Shmulevich, C. Sander, J. M. Stuart, Cancer Genome Atlas Research Network, et al. The cancer genome atlas pan-cancer analysis project. *Nature genetics*, 45(10):1113, 2013.
- L. Wilkinson. Dot plots. *The American Statistician*, 53:276–281, 1999.
- L. Wilkinson and M. Friendly. The history of the cluster heat map. *The American Statistician*, 63(2):179–184, 2009.
- D. P. Woodruff. Sketching as a tool for numerical linear algebra. *arXiv:1411.4357*, 2014.
- Y. Xie, P. Chenna, J.S. He, L. Le, and J. Planteen. Combining automated analysis and visualization techniques for effective exploration of high-dimensional data. In *2009 IEEE Symposium on Visual Analytics Science and Technology*. IEEE, 2009.
- Y. Xie, P. Chenna, J.S. He, L. Le, and J. Planteen. Visualization of big high dimensional data in a three dimensional space. In *2016 IEEE/ACM 3rd International Conference on Big Data Computing Applications and Technologies (BDCAT)*. IEEE, 2016.

J. Zhang and M. Huang. 2d approach measuring multidimensional data pattern in big data visualization. *2016 IEEE International Conference on Big Data Analysis (ICBDA)*, pages 1–6, 2016.

H. Zou, T. Hastie, and R. Tibshirani. Sparse principal components. *Journal of Computational and Graphical Statistics*, 15:265–286, 2006.